An In-Situ Soil Moisture Sensor Array for Real-Time Soil Moisture Depth Sensing.

Edward Munns
Curtin University
Perth, Australia
18871773@student.curtin.edu.au

***Abstract*—Moisture seeking is an optimization technique which can be implemented during sowing operations to improve crop establishment and harvest yield outcomes for cereal crop growers in the agricultural sector. In moisture seeking, the depth seed is placed in the soil profile is increased to place seed at a soil layer with sufficient moisture for germination to begin immediately after sowing. This work examined the viability of a soil moisture sensor array designed to be incorporated into the feedback loop of a sowing depth control system during moisture seeking operations. The work identified high purity alumina as a material that could be capable of withstanding the abrasive environment of this sensing domain and 0.5 mm alumina shields were incorporated into the design and tested. Finite Element Analysis demonstrated the technique of electrode mirroring could provide substantial improvement to sensor response. Finally, an attempt at characterization of the sensor array demonstrated the design was capable of sensing changes in soil moisture through the alumina shield and the variance between sensors in the array displayed highly correlated linear fits.**

I. Introduction

In recent years, the widespread adoption of minimum tillage sowing systems in the Australian agricultural industry has enabled the use of a crop sowing optimization method known as moisture seeking. In moisture seeking, seed placement depth is adjusted downwards in the soil profile to place seed at a soil layer containing with enough moisture for seed germination to begin immediately after planting and crop emergence dates to be predicted with a high level of confidence. Adjustment of end effectors that allow control of seed depth placement on planting machines currently needs to be performed manually and can be a time-consuming operation. This work examines the viability of a sensor array targeted towards automating this process with a focus on fulfilling the electromagnetic requirements this application demands.

II. Literature review

This work began with an in-depth review of the current literature. The purpose of this review was to establish the current state and trends of soil moisture sensing, to identify technologies applicable to the real-time, in-situ requirements of this application, and to identify related works this research could build upon.

Yu et al published a review of soil moisture sensing technologies and research in 2021. In this review weight, tensiometer, neutron probe, gamma-ray, infra-red, and dielectric soil moisture sensing methodologies were examined. A summary of the major findings of previous studies into many commercially available sensors was included in this review. Capacitive sensors were identified as providing major cost benefits over time domain reflectometry devices, but the review also highlighted the importance of correction algorithm optimization in providing accurate measurements. Factors affecting accuracy of capacitive sensors identified include installation method, temperature drift, soil type, ionic conductivity and unoptimized or inappropriate algorithms [1].

Escriba et al developed a co-planar soil sensor capable of sensing both soil salinity at lower frequency (300-1000 kHz) and soil moisture at higher frequency (4-10 MHz) by switching of the oscillation sources providing excitation to the sensor. This design was based on a traditional co-planar capacitor (CPC) design with electrodes arranged in a novel double helix layout. Results showed dissolved Ionics present in the material under test (MUT) lead to high variability of moisture readings at lower frequencies with these readings converging at higher frequencies. This work also examined the effects of including a polymer layer encasing the sensor to provide mechanical shielding. This shielding demonstrated a constant increase in measured capacitance across the 10-60% soil moisture range of an estimated 14.7pF and an overall reduction in sensor sensitivity of 12% due to the additional parasitic capacitance introduced by this layer [2].

Claudel et al presented an analytical method for optimization of interdigital capacitive (IDC) sensors. Results of this method were validated against finite element analysis simulations. This study demonstrated penetration depth and bandwidth were largely dependent upon electrode and inter-electrode gap widths [3].

Patle et al developed a sensor array consisting of 5 sensors placed at 5 cm increments over a 25 cm soil depth profile. These sensors were IDCs constructed on a 2-layer PCB with the IDC electrodes mirrored on both sides of the PCB. This mirroring of the electrodes demonstrated a tripling of capacitance compared to earlier works with an average ΔC of 300pF across the 5 sensors. The design used time domain multiplexing to iterate through all sensors in the array over a 250ms period with output signals fed into a counter to convert capacitance to pulse rate [4].

Kim, Chae and Nishigaki developed a method of compensating for air content present in soil pores using ethanol injection. This ethanol displaced air in samples and FDR measurements were taken at a frequency of 1 GHz. The method presented allows for the estimation of effective and

physical porosities in saturated soils by calculation of total permittivity estimates from known permittivity values of soil component materials and the ratios of these materials in the sample [5].

Finlay and Howard iteratively developed prototypes of 1, 3, and 36 row crop sowing machines featuring a semi-autonomous real-time depth control system implemented with hydraulic actuators and using an array of soil moisture sensors to provide system feedback. Field trials were performed across multiple growing seasons beginning with the single tine prototype. This design was trailer mounted and towed by a utility vehicle. The trial tested various sensor types and helped to refine the hydraulic control system. A major limitation of this trial was that the single row rendered concurrent testing of multiple sensors impossible. The 3-tine prototype was mounted on a small agricultural tractor. In this trial the hydraulic system was supplied by the tractor. The higher tine count allowed for concurrent testing of multiple sensors but increased the actuation system complexity significantly as actuators also had to be controlled concurrently. Pressure and load sensors were incorporated to provide data of forces in tines at variable tillage depths. The latest trial occurred in 2023 with the 36-row design. The 36 sowing tines were mounted on a 12-meter frame for full-scale testing of the system. The parallel compute requirements due to the high tine count made control software a challenge. Objectives of the project in 2024 include implementing system control over ISOBUS, further in-field trials and the development of a new sensor to improve accuracy and wear resistance [6].

Sulek and Ogorkiewicz analyzed the effects of sowing depth and seed size on germination quality and harvest yield of wheat plants. Sowing depths of 1 cm, 3 cm, 5 cm, and 7 cm and seed size classes of small (1.8-2.2 mm), medium (2.2-2.5 mm), and large (>2.5 mm) were evaluated on germination time and germination percentage. Results showed higher germination rates with the large seed group, the 5 cm and 7 cm deep sowing delayed germination and reduced germination rate, and the optimal group was the large seed with 3 cm sowing depth [7].

Rego Segundo et al presented a method of approximating complex permittivity using a current-to-voltage conversion circuit and dual frequency amplitude measurement. This method had the benefit of not requiring phase measurement of signals, leading to lower component speed requirements and lower complexity of circuits compared to the traditional method of measuring both amplitude and phase of signals. Results demonstrated maximum error of 0.6% for electrical conductivity measurement and maximum error of 2% for relative permittivity measurement [8].

III. Background

A. Nill-till Sowing Systems

As of 2016, over 74% of the Australian cereal crop is sown with systems referred to in the industry as “minimum till” or “nill-till” [9]. These systems have largely replaced the traditional “full-cutout” sowing method where tillage points were designed to till soil in a shallow, wide pattern with the intention of maximizing mechanical control of weed species during sowing. Minimum tillage systems instead cut narrow, deep slots into the soil at wider row spacings and allow far greater control of seed and fertilizer placement in the soil depth profile. An example of a nill-till sowing system can be seen in figure 1. First the tillage point cuts a narrow (~15mm), deep (150-300 mm) slot into the soil. This is immediately followed by a fertilizer dropper which drops fertilizer deep into the slot in the wake created by the point. Soil is then allowed to backfill the slot, burying the fertilizer below the seed bed. An opening tool then re-opens the loose soil at a depth which can be adjusted via the two adjustment bolts shown in the figure. This is followed by a seed dropper that drops seed into the re-opened slot at the depth set by the opening tool. Finally, a press wheel is rolled over the slot burying the seed. The whole seed placement assembly rides on this press wheel and moves independent of the tine assembly via a spring-loaded hinge that compensates for localized changes in soil height and keeps the sowing depth constant [10].

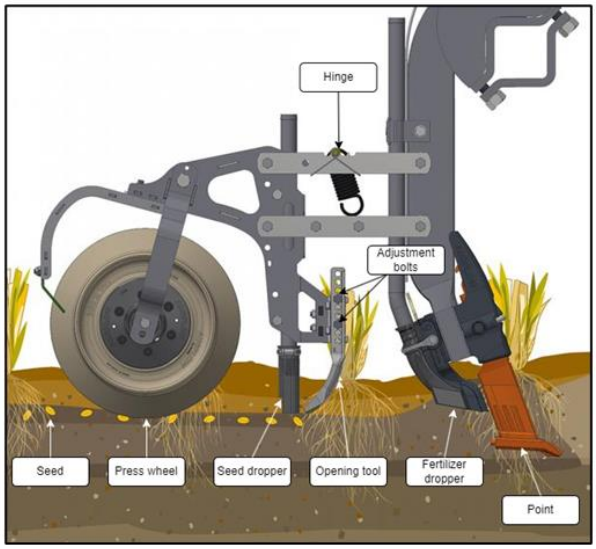

Figure 1: Nill-Till Sowing System [10].

B. Moisture Seeking to Optimize Crop Emergence

Cereal crops can be either wet sown or dry sown. Wet sowing is performed when soil moisture is at a level which allows the germination process to begin immediately after sowing and seedling emergence times and plant flowering windows can be predicted with a high level of confidence. In dry sowing, seed is placed at a layer in the soil with insufficient moisture levels for germination, so seed lays dormant until the next rainfall event. The predictable nature of wet sowing makes it the preferred method, however the large areas that need to be covered during sowing operations in the Australian cropping industry means a significant percentage of the national crop is normally dry sown out of necessity [11].

The greater control of seed and fertilizer placement due to the wide-spread adoption of nil-till sowing systems has enabled a crop emergence optimization technique known as moisture seeking. In moisture seeking, seed is placed deeper in the soil profile at a soil layer with sufficient moisture to allow germination to begin immediately after sowing, in conditions where traditional sowing systems could only dry sow. While sowing operations are performed at the beginning of a season,

it is important to note that the critical factor moisture seeking can optimize occurs at the end of a season. By increasing the reliably with which the crop emergence date can be predicted, the flowering window of a specific crop variety can be placed appropriately. Flowering too early in a season increases the risk of crop damage due to frost events, and flowering too late can lead to yield loss due to low moisture levels and temperature increases late in spring. These factors can have significant effects on yield outcomes for stakeholders in this industry [12].

C. Capacitive Sensors in Soil Moisture Applications

The most common form of capacitator is the parallel plate capacitor (PPC) where electrodes are conductive plates on parallel planes with a dielectric material placed between them. The capacitance of a PPC can be approximated by (1),

$$C = \boldsymbol{\varepsilon}\frac{A}{d} \tag{1}$$

where $\boldsymbol{\varepsilon}$ is the complex permittivity of the dielectric, A is the area of the electrode plates and d is the distance between the plates. Note in this equation capacitance is a function of the complex permittivity of the dielectric and a geometric constant for the case where geometry is fixed.

In many capacitive sensing applications, this configuration is altered from a parallel to a coplanar arrangement so the electric field can extend into the MUT above the electrodes (Figure 2). This configuration is referred to as a coplanar capacitor (CPC). Interdigital capacitors (IDC) are a subset of coplanar capacitors with electrodes consisting of a series of interleaved digits. This configuration can provide higher capacitance per area and allows for application specific tuning of sensor traits through alteration of digit width, digit count and periodicity of the electrode layout.

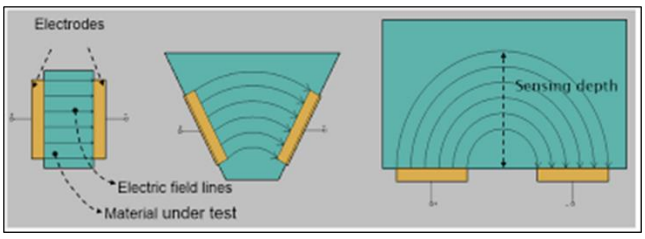

Figure 2: Parallel Plate (Left) to Coplanar (Right) Capacitor [13].

In capacitive soil moisture sensing domains, calibration is generally required to compensate for localized changes in soil properties such as soil texture, ionic content, conductivity, pH and void density. These factors can have a large influence on soil permittivity and sensor output.

D. Constraints of the Sensing Environment

To provide functionality in this application, the design discussed in this work must be capable of providing reliable readings of soil moisture of soil layers in real-time at a depth resolution of approximately 10 mm. To provide these measurements, the sensor array must be placed in contact with the soil between the point and the opening tool seen in figure 1. This environment is extremely abrasive, mechanically aggressive and the acidic nature of agricultural fertilizers mean it is also highly chemically corrosive. These constraints present significant challenges to sensor design for this appliction.

IV. Design and Development of Sensing Prototypes

A. Investigation and Initial Design Development

The challenges presented by this sensing environment are significant, so priority was placed on developing a method of dealing with these constraints. To handle the mechanical requirements the sensing elements in the array had to be protected by some form of environmental shield which was highly resistant to mechanical abrasion and chemical corrosion while also exhibiting suitable dielectric properties so sensing through the shield was possible. Metals cannot be used as a metal would negate the fringing field completely, polymers are commonly used for environmental shielding of capacitive soil sensors but lack the mechanical properties this use-case demands. Ceramics were identified as the most likely material class for construction of this shield layer. An examination of the properties, cost, and availability of ceramics identified high purity Al_2O_3 as a material that may be suitable. Al_2O_3 is widely available in pre-fabricated substrates of various thickness and purity. Substrates of 0.5, 1 and 2 mm were purchased and an initial investigation was performed on two commercially available sensors, an IDC and CPC design to compare the ability of the designs to sense through this shield layer. This investigation helped to develop an initial design (figure 3) and resulted in the development of a hypothesis that CPC sensor layouts may be more suitable than IDC sensors in this application.

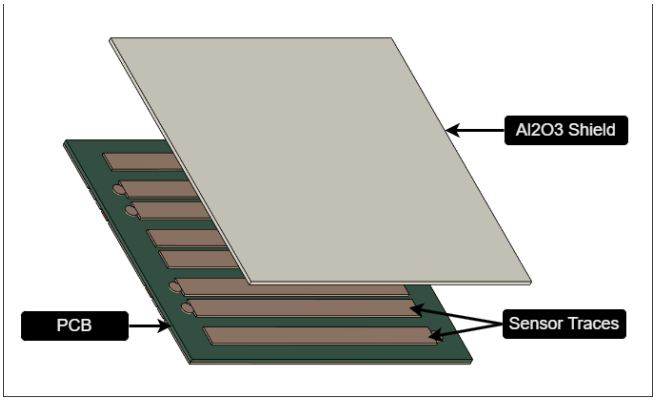

Figure 3: Initial Prototype Design.

B. Design Optimization and Prototype Fabrication

Design optimization was carried out via Finite Element Analysis (FEA) modelling with the Comsol Multiphysics electrostatics software package. The sensor array configuration and shielding requirements of this application required modelling to be performed as close to the real-world situation as possible. It was essential that simulations were performed with the shield layers in place as minimizing attenuation of the fringing fields through this shield layer was the primary target for optimization. Discussion with industry stakeholders revealed a soil depth resolution of 10 mm would be appropriate for this application. To optimize sensor

capacitance in this area, the inter-sensor space between sensors in the array had to be minimized.

Initial simulations were performed on IDC and CPC designs to confirm the hypothesis generated during the investigation phase that CPC designs were more suited to this application. This was followed by simulations of a single sided 40 mm long CPC design, a dual sided 40 mm long CPC design, and a dual sided 80 mm long CPC design. An electrode mirroring technique described by Patle et al. was implemented in the dual sided designs [4]. Comparative analysis of these results was then used to guide selection of optimization pathways appropriate for this use-case.

The configuration of the device under test (DUT) used for simulation was an array of 5 sensors implemented as copper traces on the top and bottom layers of a 2-layer PCB. Total PCB thickness was 1.6 mm, with 35-micron copper layers on top and bottom and the remainder FR4 dielectric substrate. Permittivity of the FR4 was set to 4.4 in line with manufacturer specifications [14]. A constant 2 mm spacing was used between the PCB edge and the sensor array boundary. 0.5 mm thick shield layers of Al_2O_3 with permittivity values set to 9.5 were placed over the sensor array in surface contact with the sensor electrodes. For dual sided design simulations, shield layers were placed over the sensors on both sides of the PCB, for single sided simulations the lower shield was removed, and the bottom copper layer of the PCB was used as a ground plane. The area of these shield layers was setup to automatically scale to match the dimensions of the PCB. An excitation voltage of 12 volts was used throughout simulations. The control circuitry of the design implements a Texas Instruments TMUX4052 analogue multiplexer to iterate through sensors in the array during measurement. This IC contains 2 multiplexer circuits in a single-pole 4-throw configuration, with non-active sensors left floating, not connected to ground [15]. This results in the only path to ground of the fringing field being through the output electrode of the active sensor. The input and output traces of the 4 non-active sensors in the array were therefore set to floating potential during simulation.

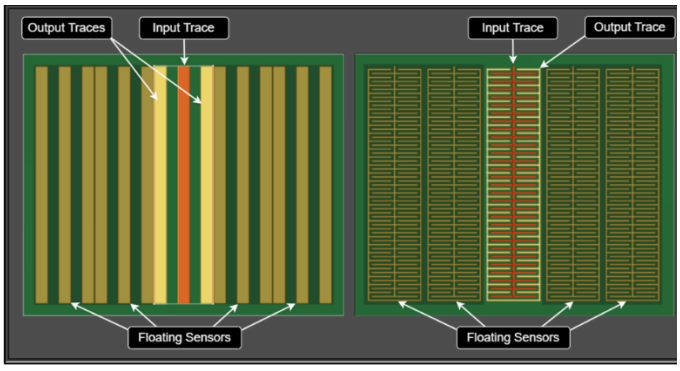

Figure 4: DUT Configuration used for Simulation.

The Comsol Electrostatics module is setup by default to calculate capacitance, total energy and magnitude of the E-Field over the entire volume of the modelling space. For this application, the attenuation of the E-Field through the FR4 and Al_2O_3 layers results in significant percentages of the total energy being present between the upper and lower bounding surfaces of the DUT. These percentages are highly dependent on sensor electrode geometry and were the primary target of optimization for this work. To quantify effective values of these parameters over variable electrode geometries the modelling space was divided into three subdomains: upper and lower MUT domains A and B, and a loss domain extending from the top to the bottom bounding surfaces of the DUT. This division of the modelling space allows separate simulation parameters to be added for each domain of the modelling space so the percentage of the E-Field present in the MUT domains can be quantified. The material of the loss domain was set to air and kept constant throughout all simulations. Separate simulations were performed with the material of the MUT domains first set to air with a real permittivity value of 1, then to water for a real permittivity value of 80. The dimensions of the modelling space was setup to automatically scale with the dimensions of the DUT so DUT to world boundary distances were kept constant throughout simulations at 10 mm in x, 20 mm in y and 40 mm in z.

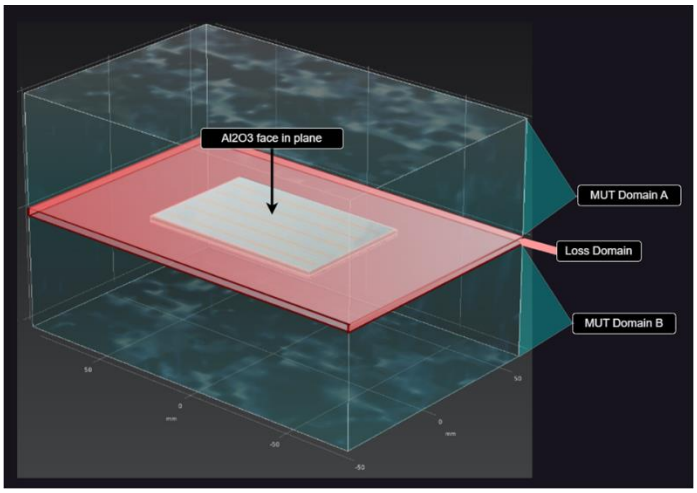

Figure 5: Division of Modelling Domains.

Optimization of design geometry was performed by running parametric sweeps of 2 geometric parameters of the sensing elements. These parameters were the width of the input and output electrodes in the case of CPC designs, and the metallization ratio and output digit count in the case of IDC designs. These parametric sweeps first update the sensor geometry, then perform the same electrostatics study in a nested for loop across all combinations of the geometric parameters. Sweeps were run twice, first with the MUT domains set to air then to water, and the results of both sweeps were combined into a single dataset containing all simulation results for the minimum and maximum MUT permittivity settings. These results was then used to evaluate sensor optimization techniques and select a suitable design for manufacture and characterization. The primary parameters used for sensor selection were the percentage change in capacitance between the air and water sweeps and the minimum sensor capacitance.

Once a suitable design had been selected a 2D CAD file of the sensor electrodes was exported from Comsol and imported into the KiCad PCB design software and a custom sensor footprint was created. This footprint was used to design a 4-sensor array constructed on the top and bottom copper layers of a 4 layer PCB to use for sensor characterization.

C. Characterization of Prototype

An initial attempt at characterization of the sensor array was performed to evaluate the ability of the design to function in this application. Many soil properties can affect the output of capacitive sensors, so the scope of this experiment needed to be limited to allow testing of a single soil feature. Soil clay content was identified as a parameter that can have a large impact on sensor output [16], so testing was performed across a series of clay and sand mixtures. The soil texture tringle (Figure 5) was used to select ratios of sample appropriate for this application. Refined kaolinite clay was used for the clay component of the samples, and kiln dried sand was used for the sand component. The soil sample groups and their sand to clay ratios are listed in table 1.

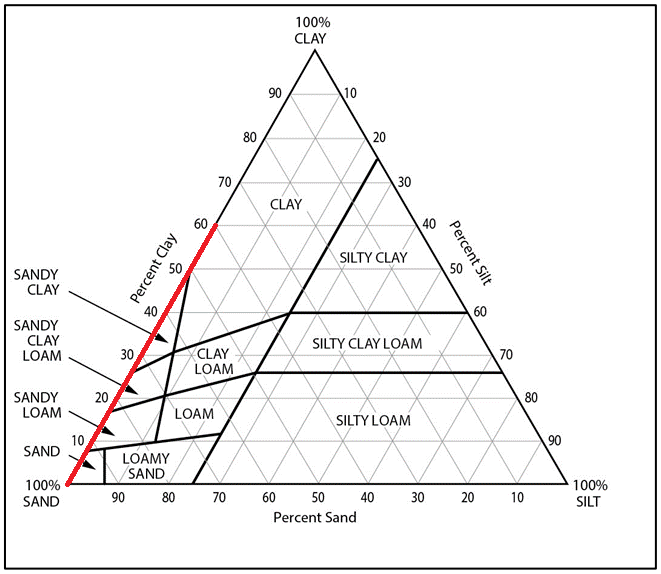

Figure 6: Soil Texture Triangle [17].

SAMPLE GROUP	SAND (%)	CLAY (%)
SAND	100	0
SANDY LOAM	80	20
SANDY CLAY	60	40
CLAY	40	60

Table 1: Clay and Sand Ratios of Characterization Samples.

For each of the 4 soil groups a 2-litre dry master mixture was created in a dedicated container. These samples were thoroughly mixed with an electric drill and grout mixing drill attachment. Once this initial mixing of the dry soil components was complete, 1 liter of the mixture was measured out and weighed on an electronic scale so the bulk density of each soil type could be calculated with (2).

$$Bulk\ Density\ (\rho_b) = \frac{Mass\ (Dry)}{Volume\ (Dry)} \qquad (2)$$

These samples were then reincorporated back into the master mixture. Measurements were taken on approximately 800 ml sub-samples taken from the center of the master mixture. Distilled water was added to the master mixture in 20 ml increments and thoroughly incorporated between each reading. The volumetric moisture content of the samples could then be calculated. This process was repeated until the samples reached the point of saturation.

A 10 MHz 5-volt peak-to-peak sine wave excitation signal was generated with a Siglent SDG2122X signal generator and output was measured with a Siglent SDS1204X-E oscilloscope. Channel 2 of the signal generator was slaved to channel 1 and connected with a coaxial cable through a 50 Ohm feed through termination resistor to channel 1 of the oscilloscope. This signal was used as a Vin reference signal so the time delay of the output signal could be measured. Channel 1 of the signal generator was connected through an SMA test fixture PCB which allowed input and output wires to be broken out for the sensor array. The output connector of this PCB was then connected through another 50 Ohm terminator to channel 3 of the oscilloscope. Measurements were taken across all 4 sensors in the array for each increase in moisture to allow the sensor-to-sensor variance to be analyzed.

V. RESULTS

A. Design Optimimization and Prototype Fabrication

The optimization stage began with a visual inspection of simulations of the E-Field performed on both a CPC and an IDC sensor design (figure 7). The top images show the E-Field of both sensors looking down from above and demonstrate the trace geometry of the DUT, while the bottom images are a cross section of the PCB and shield layers taken at the centre of the DUT. These results show the IDC design has a much higher percentage of the E-Field present in the Al_2O_3 and FR4 layers. It is also clear that because of the lower energy levels present in the loss domain of the CPC design, a larger fraction of the E-Field can extend further into the MUT. This work focused only on CPC designs after analysis of these results.

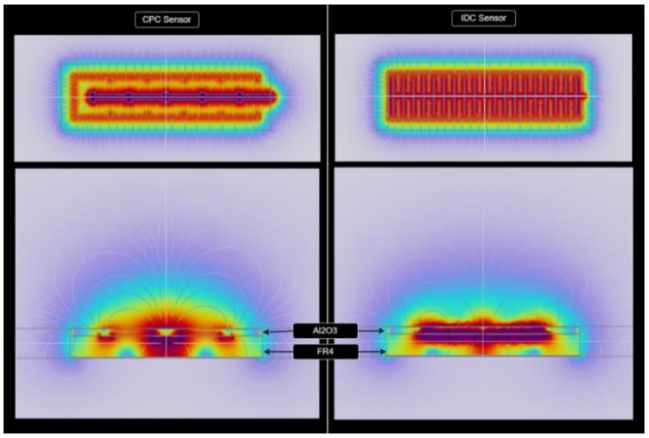

Figure 7: Comparison of E-Field for CPC (Left) and IDC (Right) Sensors.

Results of single sided and dual sided simulations for change in capacitance (figure 8), percentage change in capacitance (figure 9) and change in the magnitude of the E-Field in the MUT domain demonstrate the electrode mirror technique demonstrated by Patle et al. [4] to be a significant optimization for this application. While the increase in overall capacitance is a positive feature of this dataset, the substantial shift in the percentage change in capacitance and change in the E-Field present in the MUT will result in a large increase in the dynamic range of the sensor.

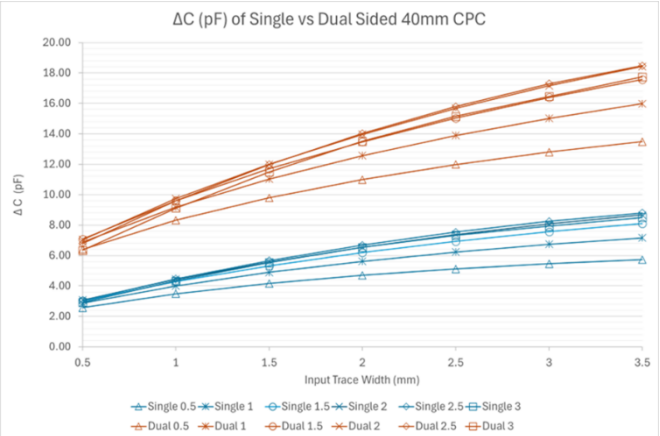

Figure 8: Change in C of Single and Dual sided 40 mm Sensors.

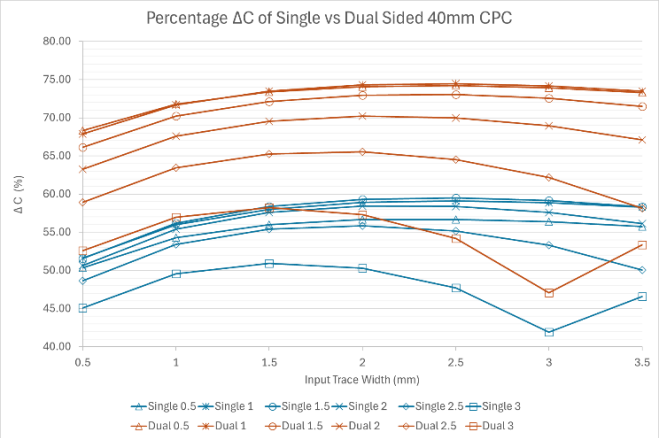

Figure 9: Percentage Change in C of Single and Dual Sided 40mm CPC.

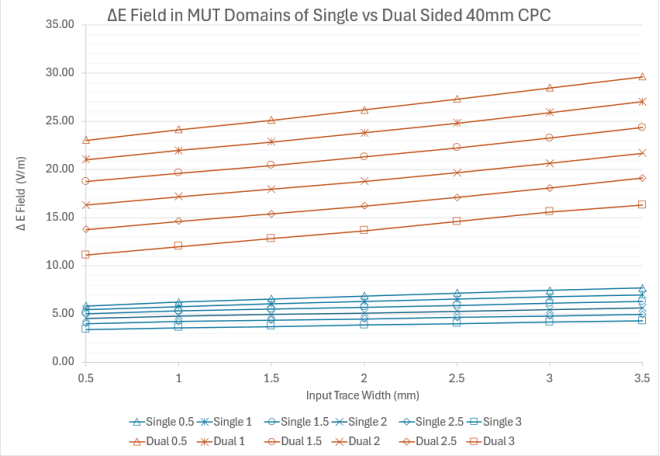

Figure 10: Change in E Field in MUT of Single and Dual Sided 40mm CPC.

Results of dual sided 40 mm vs 80 mm long sensor simulations for change in capacitance (figure 11), percentage change in capacitance (figure 12) and change in the magnitude of the E-Field in the MUT domain (figure 13) further demonstrate the optimization potential the electrode mirroring technique can provide in this application. While doubling the sensor length from 40 to 80 mm results in an approximate doubling in overall capacitance, the difference in the percentage change in capacitance and E-Field in the MUT results between these optimization methods is substantial. In both optimization methods the area of the sensor is doubled, but electrode mirroring is clearly a much more effective optimization pathway. This is likely due to the repulsive force of like charges acting through the FR4 PCB substrate repelling the fringing field out from the PCB through the alumina shields, and into the MUT.

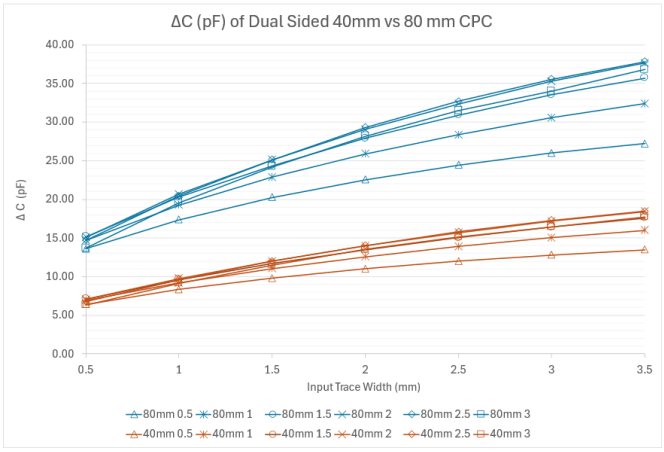

Figure 11: Change in C of Dual Sided 40mm and 80mm CPC.

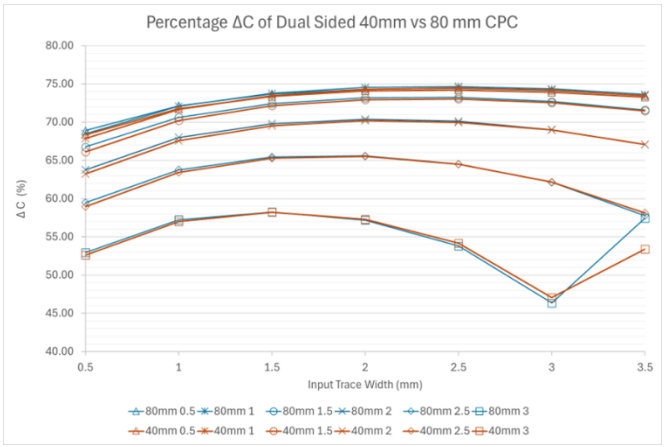

Figure 12: Percentage Change in C of Dual Sided 40mm and 80mm CPC.

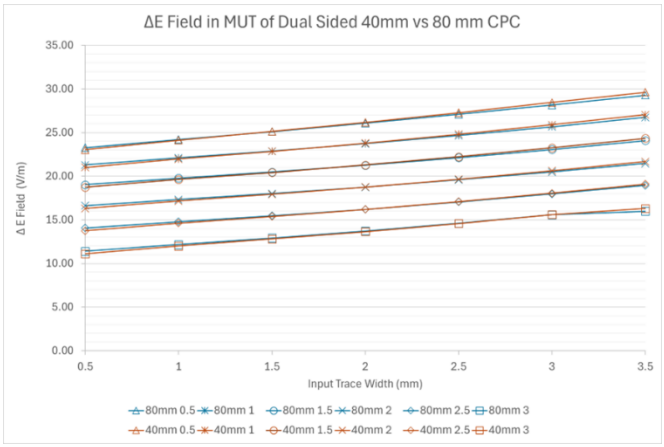

Figure 13: Change in E Field in MUT of Dual Sided 40mm and 80mm CPC.

The design chosen for the prototype was a dual sided 40 mm long CPC with a 1.5 mm input trace width and 3 mm output trace width. Simulations of this design showed a minimum capacitance of 6.21 pF in air, and a 22.6 pF maximum capacitance in water, and a percentage change in capacitance of 72.54%. This design was selected as it was within 2% of the maximum percentage change in capacitance of all designs tested and had a minimum capacitance considered suitable for characterization. The PCB for the prototype was created and

boards were manufactured for use in characterization (figure 14).

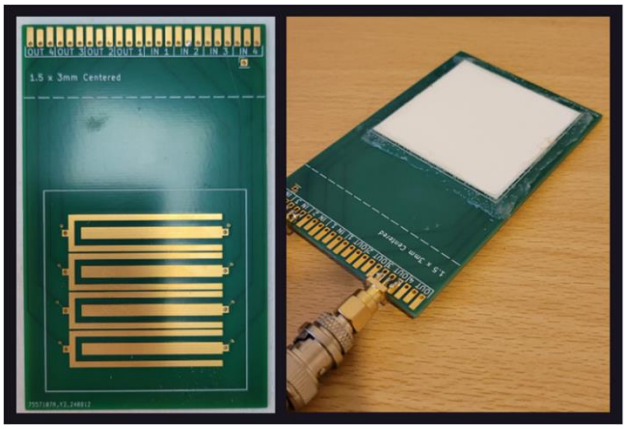

Figure 14: Prototype PCB and Assembly.

B. *Characterization of Prototype*

The results of sensor characterization (figure 15) highlighted some unforeseen factors that can have a large impact on results. The amount of water that was required to allow mixtures to be fully incorporated varied greatly between the soil series, increasing from approximately 80 ml for the sand, sandy loam and sandy clay series to 200 ml for the clay series. As the clay percentage of the samples was increased, the water and clay in the samples tended to bind into small balls which made even incorporation impossible at these moisture levels. The noise present in the clay soil series was noticed during the experiment and was likely due to wear of the sensor input cable towards the end of testing. Another source of noise in this data was identified while carrying out this experiment. The sensor must be reinserted for every measurement, resulting in inherent variability of the results due to the nature of how the samples must be prepared. The level of compaction of the soil around the sensor can change the voltage output significantly so some noise is expected when using this characterization method. While there is a great deal of noise in the clay soil series due to the connector issue discussed above, the results for the Sandy Loam and Sandy Clay datasets show linear fits with R^2 values of 0.9574 and 0.922 respectively. As the Sandy Loam soil series demonstrated the best linear fit, this series was used to examine the sensor-to-sensor variance of the prototype.

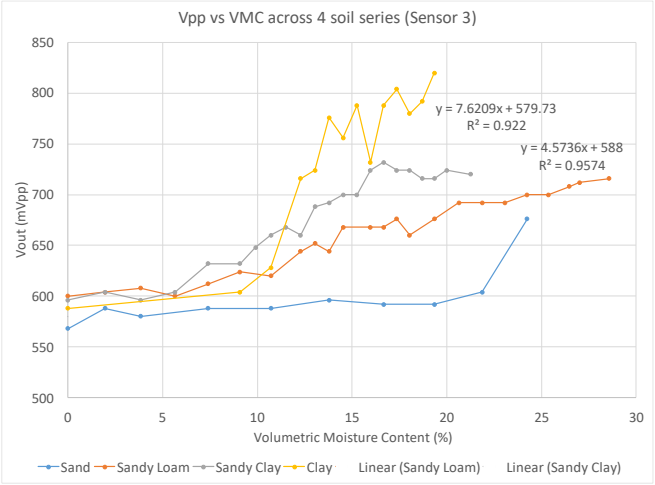

Figure 15: Results of Initial Characterization of Prototype.

Sensor-to-sensor variance results (figure 16) show linear fits which appear to be divisible into 2 distinct sub-sets based on their derivatives, with sensors 1 and 4 in one sub-set exhibiting a larger derivative than sensors 2 and 3 in a second sub-set. This was an expected feature of this data and was hypothesized during the literature review. It is also the reason that an array of 4 sensors was selected for the prototype. In the paper by Claudel et al. on the optimization of IDC sensors, the capacitance model presented uses different equations for capacitance of edge digits and internal digits to account for the lack of a conductor on one side of the edge digits [3]. It is likely a similar effect is occurring here, with the sensors at the top and bottom of the array exhibiting slightly different responses to those in the center. It's possible that the addition of copper strips at floating potential at the top and bottom of the array could result in higher correlation of the edge and internal sensors. If this method proved unsuccessful, slightly different models for internal and external sensors could be used. The shift in intercept between the sensors is likely due to the additional PCB trace length required for the sensors lower in the array, and could likely be bought into closer alignment by matching the trace length of sensor traces during PCB design.

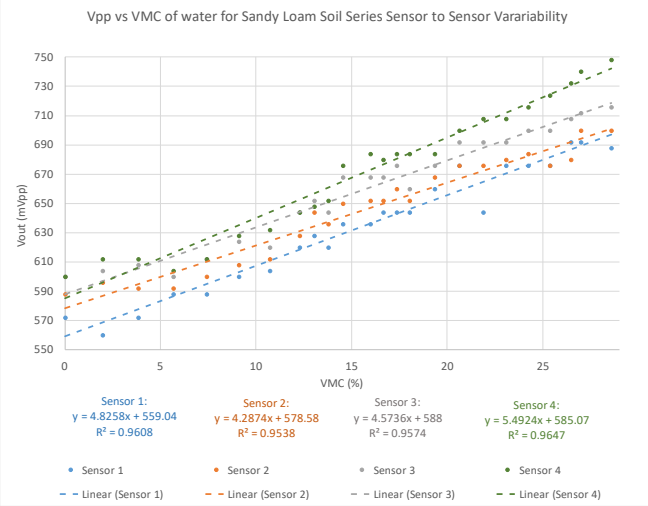

Figure 16: Sensor to Sensor Variance for Sandy Loam Soil Series.

VI. CONCLUSION

This work has presented a sensor array design that is capable of maintaining acceptable signal levels for soil moisture sensing through the 0.5 mm alumina shields, however an examination of the ability of this material to withstand the challenging mechanical constraints of this sensing environment fell outside the scope of this work. To function in this use-case it is essential a design can fulfill these mechanical requirements. The finite element analysis modelling performed during optimization of the design demonstrates the substantial gains in dynamic range that can be realized with the electrode mirroring technique demonstrated by Patle et al [4]. It's likely this optimization pathway may be effective in cases similar to this work, where penetration of environmental shielding is a requirement of a design. The characterization of the sensor array has demonstrated the design is capable of sensing changes in soil moisture and the sensor-to-sensor variance of the design exhibit positive traits for further characterization.

ACKNOWLEDGMENTS

Professor Tele Tan
Dr Julia Easton
Mr. Jayden Ng

VII. REFERENCES

[1] L. Yu, W. Gao, R. R. Shamshiri, S. Tao, Y. Ren, Y. Zhang and G. Su, "Review of research progress on soil moisture sensor technology," *International Journal of Agricultural and Biological Engineering* , pp. 32-42, 2021.

[2] C. Escriba, E. G. A. Bravo, J. Roux, J.-Y. Fourniols, M. Contardo, P. Acco and G. Soto-Romero, "Toward Smart Soil Sensing in v4.0 Agriculture: A New Single-Shape Sensor for Capacitive Moisture and Salinity Measurements.," *Sensors*, vol. 20, p. 6867, 2020.

[3] J. Claudel, A. L. Alves de Araujo, D. Kourtiche, M. Nadi and A. Bourjilat, "Optimization of Interdigitated Sensor," *Interdigital Sensors*, vol. 36, pp. 91-122, 2021.

[4] K. S. Patle, V. Panchal, R. Saini, Y. Agrawal and V. S. Palaparthy, "Temperature compensated and soil density calibrated soil moisture," *Measurements*, vol. 201, p. 111703, 2022.

[5] M.-I. Kim, B.-G. Chae and M. Nishigaki, "Evaluation of geotechnical properties of saturated soil using dielectric responses," *Geosciences*, pp. 83-93, 2008.

[6] D. Finlay and G. Howard, "Integrating soil moisture sensor technology into seeding equipment to optimise seeding depth and crop establishment," GRDC, 2024.

[7] A. Sulek and M. Ogorkiewicz, "Impact of sowing depth and seed size on the dynamics of germination and productivity of spring wheat," *Polish Journal of Agronomy*, vol. 43, pp. 63-69, 2020.

[8] A. Rêgo Segundo, É. Silva Pinto, G. Almeida Santos and P. de Barros Monteiro, "Capacitive Impedance Measurement: Dual-frequency Approach," *Sensors*, vol. 19, pp. 1-12, 2019.

[9] R. Llewellyn and J. Ouzman, "Conservation agriculture in Australia: 30 years on," 2020.

[10] Ausplow, "SOIL HEALTH AN AGENDA ITEM," 2024. [Online]. Available: https://www.ausplow.com.au/soil-health-an-agenda-item/.

[11] GRDC, "MANAGING SOIL WATER TO IMPROVE GRAIN PROFITS".

[12] Department of Primary Industries, "Western Australian Crop Sowing Guide," 2024. [Online]. Available: https://www.agric.wa.gov.au/sites/gateway/files/Crop%20Sowing%20Guide%202024%20-%20full%20guide.pdf.

[13] Y. Yang, T. Vervust, F. Bossuyt, J. Vanfleteren, G. Chiesura, G. Luyckx, J. Degrieck and M. Kaufmann, "Non-destructive evaluation of an infusion process using capacitive sensing technique," in *Emerging Technologies in Non-Destructive Testing VI*, 2015, pp. 293-297.

[14] JLCPCB, "PCB Manufacturing & Assembly Capabilities," 2024. [Online]. Available: https://jlcpcb.com/capabilities/pcb-capabilities.

[15] Texas Instruments, "TMUX405x Datasheet," 2024. [Online]. Available: https://www.ti.com/lit/ds/symlink/tmux4052.pdf.

[16] X. Dong and Y.-H. Wang, "The Effects of the pH-influenced Structure on the Dielectric Properties of Kaolinite–Water Mixtures," *Soil Science Society of America Journal*, vol. 72, pp. 1532-1541, 2008.

[17] Queensland Government, "Soil texture," 2024. [Online]. Available: https://www.qld.gov.au/environment/land/management/soil/soil-properties/texture.